Photolysis of Aqueous H 2 O 2 : Quantum Yield and Applications for Polychromatic UV Actinometry in Photoreactors

ARTICLE *in* ENVIRONMENTAL SCIENCE AND TECHNOLOGY · DECEMBER 2007

Impact Factor: 5.33 · DOI: 10.1021/es071379t · Source: PubMed

4 AUTHORS, INCLUDING:

Sara Goldstein
Hebrew University of Jerusalem
151 PUBLICATIONS **5,992** CITATIONS

SEE PROFILE

Joseph Rabani
Hebrew University of Jerusalem
198 PUBLICATIONS **5,073** CITATIONS

SEE PROFILE

Environ. Sci. Technol. **2007**, *41,* 7486−7490

Photolysis of Aqueous H_2O_2: Quantum Yield and Applications for Polychromatic UV Actinometry in Photoreactors

SARA GOLDSTEIN,*,† DORIT ASCHENGRAU,‡ YISHAY DIAMANT,‡ AND JOSEPH RABANI†

Department of Physical Chemistry, The Hebrew University of Jerusalem, Jerusalem 91904, Israel, and Atlantium Illuminating Water Technologies, Har Tuv Industrial Park 99100, Israel

Methanol is used to measure the yield of •OH radicals produced in the photolysis of H_2O_2 in aqueous solutions. The UV photolysis of H_2O_2 generates •OH radicals, which in the presence of methanol, oxygen, and phosphate buffer form formaldehyde, namely, $\Phi(HCHO) = \Phi(•OH)$. The quantum yield of •OH has been redetermined in view of literature inconsistencies resulting in $\Phi(•OH) = 1.11 \pm 0.07$ in the excitation range of 205−280 nm. The constancy of $\Phi(•OH)$ and the ease and sensitivity of the formaldehyde product analysis makes the H_2O_2/CH_3OH system suitable for polychromatic UV actinometry. In addition, the relatively low cost of the main components and the possibility of destroying the methanol before disposal qualify the system for both monochromatic and polychromatic actinometry in a large volume of water. The H_2O_2/CH_3OH system was applied in different commercial UV photoreactors.

Introduction

UV photolysis is rapidly becoming a useful tool for drinking water disinfection and decontamination. Disinfection is based on the photochemical destruction of DNA, thus damaging the ability of microorganisms to multiply. Decontamination of drinking water is by far less efficient. Nevertheless, systems with appropriate UV absorption and photochemistry can be in some cases treated by direct photolysis or indirectly in the presence of solutes such as H_2O_2 or ozone, which upon photolysis produce the highly reactive •OH radicals. Chemical actinometry is commonly used in photochemistry as a relatively simple and accurate method for radiation measurement (*1*). Knowledge of the light dose is useful not only for understanding the photochemistry in laboratory tests but also for testing industrial reactors. Such tests may serve as indicators for the reactors' performance and can be used for measurements of total light dose inside the reactor as well as comparing various photochemical reactors and their components. An appropriate actinometer for UV photoreactors should be based on water-soluble photosensitive chemicals, which are sufficiently stable and allow accurate and sensitive product analysis. In order to qualify for large flow rates accumulating as much as several meters[3] per test, the actinometer materials have to be reasonably cheap and either environmentally friendly or at least susceptible to photomineralization down below the toxicity limit. Common actinometers that have been used in studies of UV photoreactors include potassium ferrioxalate (*2*), potassium peroxodisulfate/*tert*-butyl alcohol (*3*), iodide−iodate (*4*), uridine (*5*, *6*), and (*E*)-5-[2-(methoxycarbonyl)-ethenyl]cytidine (*7*). However, the ferrioxalate is sensitive to room light and also introduces "noise" when applied to UV light sources also emitting higher wavelengths (*8*, *9*). The potassium peroxodisulfate/*tert*-butyl alcohol with continuous O_2 bubbling is based on $[H^+]$ measurement, where $\Phi(H^+)$ has only been determined as 1.8 ± 0.1 at 254 nm (*3*). The use of 0.6 M iodide and 0.1 M iodate (*10*) makes this actinometer less useful for large volume of water. Therefore, a technique was developed where small quartz vessels filled with the actinometric solution are positioned at various sites within the reactor (*10*). This technique has been tested only for monochromatic light at 254 nm. The relatively high optical absorption of the photoproduct makes this actinometer less useful above 280 nm. The quantum yield of uridine is only 0.02 and is dependent on the light intensity (*5*, *6*). (*E*)-5-[2-(Methoxycarbonyl)ethenyl]cytidine is not commercially available and has a relatively high optical absorption above 300 nm (*7*).

The present study concerns the use of an actinometer solution containing H_2O_2 and CH_3OH in aerated aqueous solutions containing phosphate buffer. The UV photolysis of H_2O_2 generates •OH radicals, which react with CH_3OH, forming $•OOCH_2OH$ in the presence of oxygen. The unimolecular decomposition of $•OOCH_2OH$ to HCHO and $HO_2•$ is base-catalyzed (*11*) and is the main pathway in aerated solutions containing HPO_4^{2-} and OH^-, namely, $\Phi(HCHO) = \Phi(•OH)$. The ease and sensitivity of the formaldehyde product analysis, the relatively high $\Phi(•OH)$ value, and the relatively low cost of the main components make the H_2O_2/CH_3OH system suitable for UV monochromatic and polychromatic actinometry, especially in large volumes of water. It was important at first to establish $\Phi(•OH)$ as a function of excitation wavelength in view of the large variation of the literature results (*12*−*20*). The effect of the experimental conditions such as the concentration of H_2O_2 and CH_3OH, pH, and flow rate is discussed on the basis of the known chemistry of the system and is applied in industrial UV photoreactors.

Experimental Section

Materials. All chemicals were of the highest available purity. Solutions were prepared with deionized water, which was purified using a Milli-Q water purification system for laboratory tests. Tap water, which passed active carbon filtration followed by reverse osmosis, was used for meter[3] flow tests with industrial photoreactors. The concentration of H_2O_2 (30% w/v Frutarom, Ltd.) was determined from its optical absorption using $\epsilon_{240} = 38.1\ M^{-1}\ cm^{-1}$ (*20*). The concentration of formaldehyde was determined using the Nash reagent (2 M ammonium acetate, 0.05 M acetic acid, 0.02 M acetylacetone) (*21*). The reagent was mixed with an equal volume of the tested solution, and after incubation for about 15 min at 50 °C, the concentration of formaldehyde was determined from its absorption using $\epsilon_{412} = 7700\ M^{-1}\ cm^{-1}$ (*22*). Because CH_3OH is slowly oxidized by H_2O_2 at high concentrations, the two materials were mixed shortly before the photolysis and control experiments were always carried out for thermal methanol oxidation. An excess of H_2O_2 was

* Corresponding author phone: 972-2-6586478; fax: 972-2-6586925; e-mail: sarag@vms.huji.ac.il.
† The Hebrew University of Jerusalem.
‡ Atlantium Illuminating Water Technologies.

10.1021/es071379t CCC: $37.00
Published on Web 10/06/2007

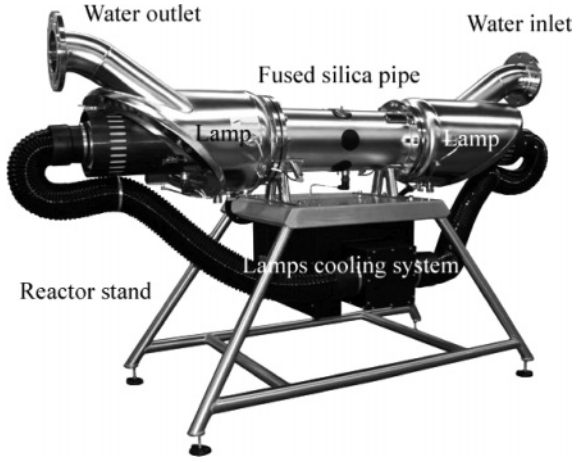

FIGURE 1. R-200 reactor. Water flows in through one of the inlet/outlet pipes and exits at the other. The medium-pressure high-intensity lamps are positioned inside the metal frame on both sides and serve as the light sources. They are separated from the flowing water by means of appropriate fused silica windows, which are positioned at a distance from the fused silica pipe (at the center) to allow the water in and out.

destroyed with catalase (EC 1.11.1.6, Boehringer-Mannheim) before the addition of the Nash reagent.

Quantum Yields Measurements. Photolysis was carried out in a cylindrical cell (2 cm i.d., 2 cm length) made from Suprasil quartz under magnetic stirring at room temperature (24 ± 1°C). The light entered through a flat optical window. The cell had a short side arm with glass taper joint, through which the solutions were introduced. A small stirrer was placed in the solution outside the light beam. The following two light sources were used: (i) A monochromatic low-pressure mercury lamp (Heraeus NNI 120/44U, with the 185 nm line filtered out). The monochromatic light passed through a 10 cm long tube located between the lamp and the sample. (ii) A xenon lamp (Osram 150W ozone free) coupled with a monochromator (SX-17MV setup from Applied Photophysics). Appropriate narrowband interference filters (10−12 nm, 14−22% peak transmittance) were used at 205, 214, 240, 253.7, 260, 270, and 280 nm. The incident light dose rate was determined using the iodide−iodate actinometer, which was prepared daily and contained 0.6 M potassium iodide and 0.1 M potassium iodate in 0.01 M $Na_2B_4O_7$·12 H_2O at pH 9.25.(*10*) The concentration of I_3^- was calculated using $\epsilon_{352} = 27\ 600\ M^{-1}\ cm^{-1}$ in the presence of 0.6 M iodide (*10*). Recently (*23*), we redetermined the quantum yields of I_3^-, and the values used in the present study are 0.92 at 205−240 nm, 0.72 at 253.7 nm, 0.53 at 260 nm, 0.42 at 270 nm, and 0.36 at 280 nm. The light absorbed by H_2O_2 solutions was calculated using Beer's law. At the higher wavelengths, the absorption of the solutions was measured using 4 or 10 cm cells.

Reactor System. Aerated stock solutions containing various concentrations of H_2O_2, 0.37 M CH_3OH, and 0.04 M phosphate buffer were injected at a constant rate of 8.5 L/min into water flowing at about 20 m^3/h. The exact flow rate was determined by measuring the concentration of H_2O_2 in the injection tank and after the mixing at the entrance to the reactor. The water flew through three different Atlantium's reactors, R-100 and two types of R-200. The scheme of the R-200 reactor is shown in Figure 1. The R-100 reactor is 75 cm long with a 10.4 cm diameter, and the R-200 reactor is 75 or 150 cm long with 16.3 cm diameter. The medium-pressure high-intensity lamp power was 1.6 and 4.2 kW in the R-100 and R-200, respectively. Two lamps were used at the same time for most of the experiments. H_2O_2 was added to the injection tank just before the experiment to minimize the thermal oxidation of CH_3OH. The solution taken at the entrance of the reactor was used as a reference for the determination of HCHO concentration. Samples were taken for HCHO analysis about 1 min after beginning the injection of the stock solution into the flowing water. The reported values are the average of at least four samples for each set of experiments. The standard deviation was less than 2%.

Results and Discussion

Mechanism and Quantum Yields in the Photolysis of Aqueous H_2O_2. The detailed reaction mechanism of the formation of HCHO is given by reactions 1−6. The •OH radicals were produced upon H_2O_2 photolysis abstraction of an H atom from H_2O_2 (reaction 2) and CH_3OH (reaction 3). The latter reaction produces $•CH_2OH$ and a small fraction of $CH_3O•$ (*24*), which is quickly converted into $•CH_2OH$ through a 1,2-H shift (not included in the reaction scheme). $•CH_2OH$ reacts with O_2 to form the respective peroxyl radical (reaction 4), which decomposes into HCHO and superoxide ($O_2^{•-}$/$HO_2•$) in a process which is base-catalyzed (reactions 5 and 6) (*11*).

$$H_2O_2 \xrightarrow{h\nu} 2•OH \quad (1)$$

$$•OH + H_2O_2 \rightarrow O_2^{•-} + H^+ + H_2O \qquad k_2 = 2.7 \times 10^7\ M^{-1}\ s^{-1}\ (25) \quad (2)$$

$$•OH + CH_3OH \rightarrow •CH_2OH + H_2O \qquad k_3 = 9.7 \times 10^8\ M^{-1}\ s^{-1}\ (25) \quad (3)$$

$$•CH_2OH + O_2 \rightarrow •OOCH_2OH \qquad k_4 = 4.5 \times 10^9\ M^{-1}\ s^{-1}\ (25) \quad (4)$$

$$•OOCH_2OH + HPO_4^{2-} \rightarrow HCHO + O_2^{•-} + H_2PO_4^- \qquad k_5 \approx 2 \times 10^6\ M^{-1}\ s^{-1}\ (25) \quad (5)$$

$$•OOCH_2OH + OH^- \rightarrow HCHO + O_2^{•-} + H_2O \qquad k_6 = 1.8 \times 10^{10}\ M^{-1}\ s^{-1}\ (25) \quad (6)$$

$$O_2^{•-} + HO_2^• (+ H^+) \rightarrow O_2 + H_2O_2 \quad (7)$$

The rate of the dismutation of superoxide ($pK_a = 4.8$) is highly pH-dependent and is also catalyzed by metal impurities (*26*, *27*). At high pH, the basic form of H_2O_2 (pK_a = 11.7 (*28*)) reacts with •OH radicals much faster (*25*, *29*), so considerably higher concentrations of CH_3OH are required. In addition, the mechanism changes due to the formation of $O_3^{•-}$ via the reaction of $O^{•-}$ with O_2 ($pK_a(•OH) = 11.9$ (*30*−*32*)) (*25*). The base-catalyzed reactions 5 and 6 compete with the second-order reactions 8 and 9, which produce HCOOH (*33*) and $HOOCH_2OH$, respectively. The latter reactions are suppressed at low intensity and high base concentration. Under the conditions where reaction 8 can be neglected, the yield of HCHO equals that of •OH because $HOOCH_2OH$ formed in reaction 9 decomposes to HCHO and H_2O_2 (*34*).

$$2•OOCH_2OH \rightarrow \text{products} \qquad 2k_8 = (0.4-2.2) \times 10^9\ M^{-1}\ s^{-1}\ (25) \quad (8)$$

$$•OOCH_2OH + O_2^{•-} \rightarrow HOOCH_2OH + O_2 \quad (9)$$

The quantum yield of HCHO was determined from the slope of the line obtained by plotting the yield of HCHO as a function of the absorbed light dose. The competition of

TABLE 1. Φ(•OH) at 253.7 nm[a]

$[CH_3OH]$, M	$[H_2O_2]$, M	Φ (•OH)
0.005	0.005	1.14 ± 0.03[b]
0.005[d]	0.005	1.10 ± 0.02[b]
0.01	0.005	1.21 ± 0.02[b]
0.05	0.005	1.14 ± 0.02[b]
0.05	0.009	1.18 ± 0.01[b]
0.20	0.005	1.21 ± 0.02[b]
0.20	0.005	1.12 ± 0.01[b]
0.20	0.009	1.21 ± 0.02[b]
0.30	0.005	1.22 ± 0.01[b]
0.40	0.010	1.08 ± 0.02[b]
0.50	0.005	1.12 ± 0.04[b]
	average	1.16 ± 0.05[c]

[a] All experiments were carried out in the presence of 2 mM phosphate buffer at pH 7.0 ± 0.2. [b] Maximum observed deviation. [c] Standard deviation. [d] With interference filter.

TABLE 2. Φ(•OH) as a Function of Excitation Wavelength

λ, nm	Φ(•OH) this study[a]	Φ(•OH) literature
200		0.72−0.76 (radiometry) (*35*)
205	1.14 ± 0.05[b]	
214	1.08 ± 0.03[b]	
222		0.90 ± 0.12 (ferrioxalate) (*36*)
240	1.12 ± 0.05[b]	
248		0.88 (radiometry) (*35*)
		1.0 ± 0.1 (radiometry) (*19*)
253.7	1.17 ± 0.09[b]	
253.7[d]	1.15 ± 0.05[c]	0.98 ± 0.05 (uranyl oxalate) (*12*)
		0.98 ± 0.13 (radiometry) (*13*)
		1.08 ± 0.10 (monochloroacetic acid and uranyl oxalate) (*15*)
		1.84 (uranyl oxalate) (*16*)
260	1.11 ± 0.05[b]	
270	1.07 ± 0.04[b]	
280	1.04 ± 0.04[b]	
308		0.8 ± 0.2 (radiometry) (*19*)
		0.98 ± 0.03 (radiometry) (*18*)
313		0.6 (radiometry)(*13*)
		0.98 ± 0.12 (2-nitrobenzaldehyde) (*20*)
		1.84 (uranyl oxalate) (*16*)
351		0.96 ± 0.04 (radiometry) (*18*)
300−400		0.96 ± 0.09 (ferrioxalate) (*37*)
average	1.11 ± 0.04[c]	

[a] All experiments were carried out in the presence of 5 mM CH_3OH, 5.2−5.5 mM H_2O_2, and 2 mM phosphate buffer at pH 7.0 ± 0.2. [b] Maximum observed deviation. [c] Standard deviation [d] Low-pressure mercury lamp.

H_2O_2 with CH_3OH for •OH radicals at relatively low ratios of $[CH_3OH]/[H_2O_2]$ apparently decreases the observed yield of HCHO. Therefore, appropriate corrections were carried out whenever necessary. The quantum yields of •OH obtained at 253.7 nm are summarized in Table 1, demonstrating that even 0.5 M CH_3OH does not effectively compete with the recombination of •OH radicals in the photochemical cage.

The quantum yields of •OH at different excitation wavelengths are shown in Table 2 and are compared with the literature values. Our results show no dependency of the quantum yield on excitation wavelength within the experimental uncertainty, though the literature values sometimes show a large scatter.

Thus, the H_2O_2/CH_3OH system is qualified for large-scale actinometry in the spectral range where there is still sufficient absorption by H_2O_2. The actinometer is highly soluble in water, and the concentrations can be adjusted to absorb most of the light in the range of interest. The thermal stability is fair. Although H_2O_2 oxidizes CH_3OH to HCHO in the dark, the reaction is sufficiently slow so that the system can be used if freshly prepared. The thermal reaction is noticed only

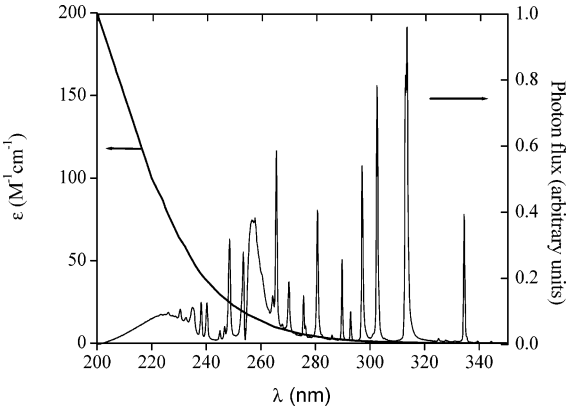

FIGURE 2. Absorption spectrum of H_2O_2 and emission spectrum of a medium-pressure Hg lamp. The extinction coefficients of H_2O_2 were taken from ref *20*. The normalized emission spectrum of the lamp was measured with a USB-2000 spectrometer, a product of Ocean Optics.

at relatively high concentrations, which are required for testing an industrial system, where a remarkable dilution takes place upon injection of the stock solution into the flowing water stream. Analysis of HCHO is sensitive because of the relatively high absorption of the adduct formed between HCHO and acetylacetone. The cost of H_2O_2 and CH_3OH, the main actinometer active components, is not prohibitive for meter[3] amounts. Although CH_3OH is not environmentally friendly, it can be mineralized in the same system by recycling the solution in the UV reactor until the CH_3OH concentration is reduced below the toxicity limit. Such operation requires control of the H_2O_2 concentration so that it is initially about the same as that of CH_3OH.

Reactor Results. The extinction coefficient of H_2O_2 is rather low and steadily decreases with increasing wavelength. The fraction of polychromatic light absorbed by H_2O_2 can be calculated from the absorption spectrum of H_2O_2 (*17*, *20*) and the emission spectrum of the polychromatic light source. The optical absorption of H_2O_2 and the emission of a typical medium-pressure Hg lamp are shown in Figure 2.

The fraction of the light absorbed at a wavelength range α is given by eq 10, where $I(\lambda)$ represent the normalized photon flux (arbitrary units) at wavelength λ, $A(\lambda) = 1-10^{-D(\lambda)}$ is the fraction of the light absorbed by H_2O_2 at λ, where $D(\lambda) = \epsilon_\lambda l[H_2O_2]$ is the absorbance.

$$\alpha = \frac{\int_{\lambda 1}^{\lambda 2} I(\lambda)A(\lambda)d\lambda}{\int_{\lambda 1}^{\lambda 2} I(\lambda)d\lambda} \qquad (10)$$

Since the quantum yield of •OH does not depend on the excitation wavelength (Table 2), and the same arbitrary units for $I(\lambda)$ are used in both the numerator and denominator, the fraction of the light absorbed by H_2O_2 in a given λ range can be easily calculated by numeric integration. Figure 3 presents a calculation of the fraction of light absorbed by H_2O_2 in two spectral ranges, namely, the germicidal light at 200−300 nm and the 300−350 nm range, as a function of $l[H_2O_2]$.

The light at 300−350 nm is not important for the inactivation of microorganisms, but nevertheless, it is partially absorbed by H_2O_2.

The absolute light density (einstein L^{-1} s^{-1}) in large volumes of water can be derived from measurements of Δ[HCHO]. The measured concentration should be divided by the fraction of the absorbed light in the wavelength range of action (will be referred to as "corrected Δ[HCHO]"). If each •OH radical leads to the formation of one HCHO molecule,

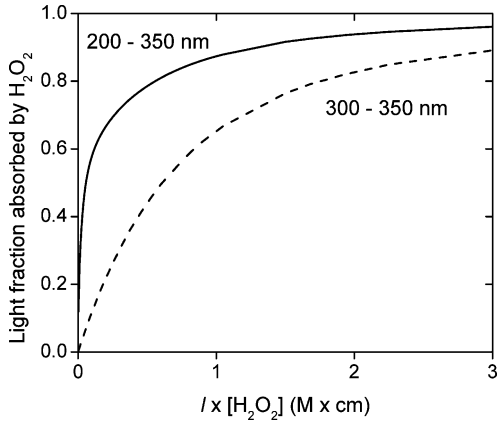

FIGURE 3. Fraction of photons absorbed by H_2O_2 at 200−350 nm and at 300−350 nm. The lines were calculated from the data of Figure 2 and eq 10, correcting for the transmission of the reactor window. The transmittance was 90% at 200−210 nm, 92% at 220 nm, 93% at 230, 94% at 250 nm, 95% at 280 nm, and 96% above 310 nm.

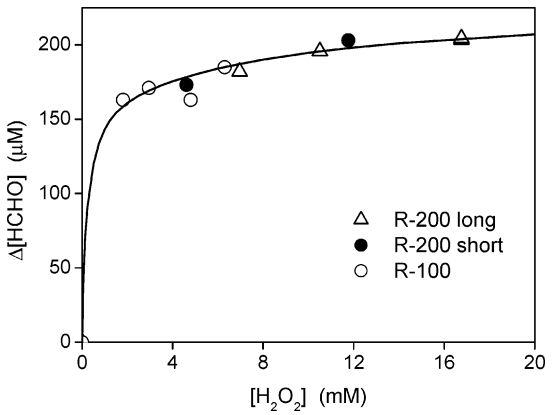

FIGURE 4. Buildup of HCHO vs $[H_2O_2]$ in the various reactors. The flowing solution contained 10 mM CH_3OH and 1 mM PB at pH 7.2. The results are normalized to a water flow rate of 20 m^3/hour. Filled circles: R-200, 75 cm long, 16.3 cm diameter, lamp power 8.4 kW. Open circles: R-100, 75 cm long, 10.4 cm diameter, Δ[HCHO] measured at or normalized to lamp power of 3.2 kW, and further multiplying by $8.15^2/5.2^2$. Triangles: R-200 reactor 150 cm long, Δ[HCHO] was normalized to the 75 cm long reactor and to lamp power 8.4 kW. The solid line was calculated for 75 cm reactors using $\Delta[HCHO]_\infty = 222\ \mu$M.

dividing the corrected Δ[HCHO] by Φ(•OH) yields the average light density. This is the case at relatively low light intensities where reactions 5 and 6 are the predominant paths for the decomposition of the peroxyl radical. At high light intensities, the contribution of reaction 9 increases due to accumulation of $O_2^{\bullet-}$ formed in reactions 5 and 6. Consequently, the yield of HCHO is hardly affected because reaction 9 leads to the formation of HCHO. However, in the presence of traces of metal impurities, which catalyze the dismutation of $O_2^{\bullet-}$ (reaction 7), the competition is predominantly between reactions 5, 6, and 8. Since reaction 8 does not produce HCHO, its concentration will be lower, depending on the light intensity.

Results in industrial UV photoreactors using the H_2O_2/CH_3OH system are shown in Figure 4. The measurements have been carried out using the R-100 and R-200 reactor models with fused silica pipes of cross-section area of 85 (75 cm length) and 209 cm^2 (75 or 150 cm length), respectively. The concentration of HCHO was halved when one lamp was shut down and was inversely proportional to the solution flow rate. The R-100 data has been normalized to the illumination time of the R-200 reactors, i.e., multiplying by $8.15^2/5.2^2$.

The solid line in Figure 4 was calculated from the measured Δ[HCHO] at $[H_2O_2] > 3$ mM in the 75 cm long reactors. The calculation was based on a total 200−350 nm light density of 200 μ einstein L^{-1} ($\Delta[HCHO]_\infty/\Phi(\bullet OH)$ which gives the best fit with both the 75 cm reactors. Assuming that $\Delta[HCHO]_\infty$ represents the concentration under limiting conditions, where reactions 5, 6, and 9 are predominant, the average light intensity of each lamp is about 100 μ einstein L^{-1}. The agreement between measured results on the R-200 reactor and the normalized results of the R-100 reactor means that the light density per centimeter^2 of the entrance window surface is the same for both reactors. This result is not surprising since the emission spectra of the lamps and the light geometries are similar, and the electricity power (8.4 and 3.2 kW, respectively) fairly closely parallels the cross-section areas. Comparative studies with different actinometry are under progress.

Under the conditions of Figure 4, at $[H_2O_2] < 2$ mM the fraction of absorbed light at 200−350 nm is lower than 70%, although the absorption fraction below 300 nm approaches 90%. Extrapolation to 100% absorption at the lower $[H_2O_2]$ value is complicated because part of the light is transmitted at low-incidence angles with respect to the fused silica surface. Such light exits through the fused silica and thus has a relatively short path. Therefore, deviations from the calculated line of Figure 4 are expected at low $[H_2O_2]$ levels. Most of the light is at sufficiently high-incidence angles and therefore becomes trapped in the water by total internal reflections. Obviously, the light density in water disinfection systems using monochromatic light at 253.7 nm (low-pressure Hg sources) can be much more easily measured.

The constancy of Φ(•OH) in the excitation range of 200−350 nm makes the H_2O_2/CH_3OH actinometer suitable for measurement of polychromatic light density. In this respect, it is superior to many other actinometers, where the product yield depends on the excitation wavelength and hence is affected not only by the light density but also by its wavelength distribution. The high sensitivity and ease of product analysis, inexpensive chemicals, high solubility, and fair stability in the dark make actinometry useful for large industrial UV disinfection and decontamination reactors. Unreacted methanol can be destroyed photolytically in the reactor by circulating the water. It should be noted that the photochemically active component H_2O_2 can be used as an actinometer also in the absence of CH_3OH in an unbuffered solution (*38*). In this case, •OH radicals are scavenged by the H_2O_2, producing superoxide radicals, which dismutate to H_2O_2 and O_2. However, measurements of O_2 formation in aerated solutions and/or consumption of H_2O_2 are less accurate compared with the determination of HCHO in the presence of CH_3OH. Buffered aqueous CH_3OH can be used as an actinometer for vacuum UV (*39*, *40*). In this case, the photolysis of water produces H• and •OH radicals, which subsequently abstract an H atom from CH_3OH. The mechanism of HCHO formation is otherwise similar to that of the H_2O_2/CH_3OH system.

The suggested actinometry does not replace biodosimetry for disinfection validation. It also does not replace dyed-microspheres actinometry, which is used to obtain the absorbed light distribution in photosensitive microspheres flowing with the water (*41*). The actinometry may be particularly useful for decontamination reactors as well as for comparative tests of different light sources and other light components in the reactor at constant light distribution, providing information as to the overall efficiency of the reactor.

Recommended Procedure for Actinometry. The concentration of CH_3OH should be higher than that of H_2O_2. The solution should be phosphate buffered. When polychromatic light is used, e.g., a medium-pressure Hg lamp,

the concentration of H_2O_2 has to be chosen so that the conditions are near the plateau of Figure 4. When monochromatic light is used, $[H_2O_2] > \epsilon^{-1}\, l^{-1}$ M assures more than 90% light absorption. In laboratory tests, the quality of the Millipore water and analytical-grade materials is usually sufficient to ensure quantitative conversion of •OH to HCHO. When applied to industrial reactors, the presence of traces of metal impurities has to be considered. If the presence of such impurities cannot be ruled out, $[HCHO]_\infty$ represents a lower limit of the light intensity.

Acknowledgments

The authors are indebted to Benzi Shoval (Atlantium) for invaluable assistance with all phases of the reactor operation.

Literature Cited

(1) Kuhn, H. J.; Braslavsky, S. E.; Schmidt, R. Chemical actinometry. *Pure Appl. Chem.* **2004**, *76*, 2105−2146.
(2) Harris, G. D.; Adams, V. D.; Moore, W. M.; Sorensen, D. L. Potassium ferrioxalate as chemical actinometer in ultraviolet reactors. *J. Environ. Eng.* **1987**, *113*, 612−627.
(3) Mark, G.; Schuchmann, M. N.; Schuchmann, H. P.; von Sonntag, C. The photolysis of potassium peroxodisulphate in aqueous solution in the presence of *tert*-butanol: a simple actinometer for 254 nm radiation. *J. Photochem. Photobiol., A* **1990**, *55*, 157−168.
(4) Rahn, R. O.; Bolton, J.; Stefan, M. I. The iodide/iodate actinometer in UV disinfection: Determination of the fluence rate distribution in UV reactors. *Photochem. Photobiol.* **2006**, *82*, 611−615.
(5) Linden, K. G.; Darby, J. L. Estimating effective germicidal dose from medium pressure UV lamps. *J. Environ. Eng.* **1997**, *123*, 1142−1149.
(6) Jin, S.; Mofidi, A. A.; Linden, K. G. Polychromatic UV fluence measurement using chemical actinometry, biodosimetry, and mathematical techniques. *J. Environ. Eng.* **2006**, *132*, 831−841.
(7) Shen, C.; Fang, S.; Bergstrom, D. E.; Blatchley, E. R. (*E*)-5-[2-(Methoxycarbonyl)ethenyl]cytidine as a chemical actinometer for germicidal UV radiation. *Environ. Sci. Technol.* **2005**, *39*, 3826−3832.
(8) Hatchard, C. G.; Parker, C. A. A new sensitive chemical actinometer. II. Potasium ferrioxalate as a standard chemical actinometer. *Proc. Roy. Soc., Ser. A* **1956**, *235*, 518−536.
(9) Demas, J. N.; Bowman, W. D.; Zalewskl, E. F.; Velapoldl, R. A. Determination of the quantum yield of the ferrioxalate actinometer with electrically calibrated radiometers. *J. Phys. Chem.* **1981**, *85*, 2766−2771.
(10) Rahn, R. O.; Stefany, M. I.; Bolton, J. R.; Goren, E.; Shaw, P.-S.; Lykke, K. R. Quantum yield of the iodide−iodate chemical actinometer: Dependence on wavelength and concentration. *Photochem. Photobiol.* **2003**, *78*, 146−152.
(11) Rabani, J.; Klug-Roth, D.; Henglein, A. Pulse radiolytic investigations of $OHCH_2O_2$ radicals. *J. Phys. Chem.* **1974**, *78*, 2089−2093.
(12) Hunt, J. P.; Taube, H. The photochemical decomposition of hydrogen peroxide. Quantum yields, tracer and fractionation effects. *J. Am. Chem. Soc.* **1952**, *74*, 5999−6002.
(13) Weeks, J. L.; Matheson, M. S. The primary quantum yield of hydrogen peroxide decomposition. *J. Am. Chem. Soc.* **1956**, *78*, 1273.
(14) Dainton, F. S. The primary quantum yield in the photolysis of hydrogen peroxide at 3130 Å and the primary radical yield in the X- and γ-radiolysis of water. *J. Am. Chem. Soc.* **1956**, *78*, 1278−1279.
(15) Volman, D. H.; Chen, J. C. The photochemical decomposition of hydrogen peroxide in aqueous solutions of allyl alcohol at 2537 Å *J. Am. Chem. Soc.* **1959**, *81*, 4141−4144.
(16) Hatada, M.; Kraljic, I.; El Samahy, A.; Trumbore, C. N. Radiolysis and photolysis of the hydrogen peroxide-*p*-nitrosodimethylaniline−oxygen system. *J. Phys. Chem.* **1974**, *78*, 888−891.
(17) Morgan, M. S.; Van Trieste, P. F.; Garlick, S. M.; Mahon, M. J.; Smith, A. L. Ultraviolet molar absorptivities of aqueous hydrogen peroxide and hydroperoxyl ion. *Anal. Chim. Acta* **1988**, *215*, 325−329.
(18) Zellner, R.; Exner, M.; Herrmann, M. Absolute OH quantum yields in the laser photolysis of nitrate, nitrite and dissolved H_2O_2 at 308 and 351 nm in the temperature range 278−353 K. *J. Atmos. Chem.* **1990**, *10*, 411−425.
(19) Yu, X.-Y.; Barker, J. R. Hydrogen peroxide photolysis in acidic aqueous solutions containing chloride ions. I. Chemical mechanism. *J. Phys. Chem. A* **2003**, *107*, 1313−1324.
(20) Chu, L.; Anastasio, C. Formation of hydroxyl radical from the photolysis of frozen hydrogen peroxide. *J. Phys. Chem. A* **2005**, *109*, 6264−6271.
(21) Nash, T. The colorimetric estimation of formaldehyde by means of the Hantzsch reaction. *Biochem. J.* **1953**, *55*, 416−421.
(22) In ref *21*, both 7700 and 8000 M^{-1} cm^{-1} are reported. We observed in independent experiments that the lower value is more appropriate.
(23) Goldstein, S.; Rabani, J. The ferrioxalate and iodide−iodate actinometers in the UV region. *J. Photochem. Photobiol., A* **2007**, in press.
(24) Asmus, K. D.; Moeckel, H.; Henglein, A. Pulse radiolytic study of the site of hydroxyl radical attack on aliphatic alcohols in aqueous solution. *J. Phys. Chem.* **1973**, *77*, 1218−1221.
(25) Mallard, W. G.; Ross, A. B.; Helman, W. P. *NIST Standard References Database 40*, version 3.0; National Institute of Standards and Technology: Gaithersburg, MD, 1998.
(26) Rabani, J.; Nielsen, S. O. Absorption spectrum and decay kinetics of O_2^- and HO_2 in aqueous solutions by pulse radiolysis. *J. Phys. Chem.* **1969**, *73*, 3736−3744.
(27) Behar, D.; Czapski, G.; Rabani, J.; Dorfman, L. M.; Schwarz, H. A. Acid dissociation constant and decay kinetics of the perhydroxyl radical. *J. Phys. Chem.* **1970**, *74*, 3209−3213.
(28) Evans, M. G.; Uri, N. Dissociation constant of hydrogen peroxide and the electron affinity of the HO_2 radical. *Trans. Faraday Soc.* **1949**, *45*, 224−230.
(29) Rabani, J. Pulse radiolysis of alkaline solution. *Adv. Chem. Ser.* **1968**, *81*, 131−152.
(30) Weeks, J. L.; Rabani, J. The pulse radiolysis of deaerated aqueous carbonate solutions. I. Transient optical spectrum and mechanism. 11. pK for OH radicals. *J. Phys. Chem.* **1966**, *70*, 2100−2106.
(31) Rabani, J.; Matheson, M. S. Pulse radiolytic determination of pK for hydroxyl ionic dissociation in water. *J. Am. Chem. Soc.* **1964**, *86*, 3175.
(32) Rabani, J.; Matheson, M. S. Pulse radiolysis of aqueous solutions of potassium ferrocyanide. *J. Phys. Chem.* **1966**, *70*, 761−769.
(33) Bothe, E.; Schulte-Frohlinde, D. The bimolecular decay of the alfa-hydroxymethylperoxyl radicals in aqueous solutions. *Z. Naturforsch.* **1978**, *33b*, 786−788.
(34) Zhou, X.; Lee, Y.-N. Aqueous solubility and reaction kinetics of hydroxymethyl hydroperoxide. *J. Phys. Chem.* **1992**, *96*, 265−272.
(35) Crowell, R. A.; Lian, R.; Sauer, M. C., Jr.; Oulianov, D. A.; Shkrob, I. A. Geminate recombination of hydroxyl radicals generated in 200 nm photodissociation of aqueous hydrogen peroxide. *Chem. Phys. Lett.* **2004**, *383*, 481−485.
(36) Loraine, G. A.; Glaze, W. H. The ultraviolet photolysis of aqueous solutions of 1,1,1-trichloroethane and hydrogen peroxide at 222 nm. *J. Adv. Oxid. Technol.* **1999**, *4*, 424−433.
(37) Sun, L.; Bolton, J. R. Determination of the quantum yield for the photochemical generation of hydroxyl radicals in TiO_2 suspensions. *J. Phys. Chem.* **1996**, *100*, 4127−4134.
(38) Nicole, I.; De Laat, J.; Dore, M.; Duguet, J. P.; Bonnel, C. Use of UV radiation in water treatment: Measurements of photonic flux by hydrogen peroxide actinometry. *Water Res.* **1990**, *24*, 157−168.
(39) Heit, G.; Neuner, A.; Saugy, P.-Y.; Braun, A. M. Vacuum−UV (172 nm) actinometry. The quantum yield of the photolysis of water. *J. Phys. Chem. A* **1998**, *102*, 5551−5561.
(40) Oppenlander, T.; Schwarzwalder, R. Vacuum−UV oxidation (H_2O−VUV) with a xenon excimer flow-through lamp at 172 nm: Use of methanol as actinometer for VUV intensity measurements and as reference compound for OH-radical competition kinetics in aqueous systems. *J. Adv. Oxid. Technol.* **2002**, *5*, 155−163.
(41) Blatchley, E. R., III; Shen, C.; Naunovic, Z.; Lin, L.-S.; Lyn, D. A.; Robinson, J. P.; Ragheb, K.; Gregori, G.; Bergstrom, D. E.; Fang, S.; Guan, Y.; Jennings, K.; Gunaratna, N. Dyed microspheres for quantification of UV dose distributions: Photochemical reactor characterization by Lagrangian actinometry. *J. Environ. Eng.* **2006**, *132*, 1390−1403.

Received for review June 10, 2007. Revised manuscript received August 14, 2007. Accepted August 16, 2007.

ES071379T